Research in Astronomy and Astrophysics, 25:015014 (12pp), 2025 January

https://doi.org/10.1088/1674-4527/ad9a34
CSTR: 32081.14.RAA.ad9a34

Study on Real-time Monitoring Method for Dust-scattered Stray Light in the Spectral Imaging CoronaGraph of the Chinese Meridian Project Phase II

Da-Yang Liu[1], Xiao-Yu Yu[1], Hong-Xin Zhang[2], Zheng-Hua Huang[1], Li-Dong Xia[1], Ming-Zhe Sun[1], Xian-Liang Mao[1], Bo-Yu Sun[1], Ning Tang[1], Hui Fu[1], Wei-Xin Liu[1], Chao Zhang[1], and Jian-Ping Han[1]
[1] Shandong Provincial Key Laboratory of Optical Astronomy and Solar-Terrestrial Environment, Institute of Space Sciences, Shandong University, Weihai 264209, China; sunmingzhe2003@126.com
[2] Changchun institute of Optics, Fine Mechanics and Physics, Chinese Academy of Sciences, Changchun 130033, China
Received 2024 October 20; revised 2024 November 28; accepted 2024 December 02; published 2025 January 8

Abstract

The dust-scattered stray light in an inner-occulted coronagraph mainly arises from dust particles on the surfaces of the objective lens. Due to the random accumulation of dust on the lens surfaces, it is challenging to monitor this type of stray light and no application can be used for its real-time monitor in the past. In this study, we provide a system and method to overcome this issue, and these have been applied to the Spectral Imaging CoronaGraph (SICG) of the Chinese Meridian Project. The method is based on the relation between the sizes of dust particles and its stray light level at the imaging plane established in the laboratory and the relation between the real size of dust particles and the occupancies on the imaging plane. To monitor the stray light levels accounted for by dusts, one needs only an image of the objective lens that can be provided by the auxiliary imaging system that specially comes with SICG. Our tests show that the errors of the method are less or about 2%, giving a strong confidence in its accuracy. It provides a handy tool to monitor the dust level of the objective lens of SICG and has significantly improved the efficiency of the pipeline of stray light control.

Key words: Sun: corona – techniques: image processing – instrumentation: miscellaneous – methods: analytical – scattering

1. Introduction

A coronagraph is an optical system specially designed to monitor the solar corona (Su 1959). It requires a careful design on the system to suppress the scattered light, in order to observe the extremely faint corona on a strong background due to the solar photosphere. An inner-occulted coronagraph is one type of this design, which has an occulter placed at the focal point of the objective lens to block the focused image of the disk of the solar photosphere. The stray light in an inner-occulted coronagraph can be categorized into two types based on its intensity variation, static stray light and dynamic stray light. Static stray light primarily includes diffractions at the edges of the coronagraph's apertures, ghost images caused by multiple reflections of the objective lens and those resulting from the microscopic surface roughness of the objective lens (Huang et al. 2023). These static stray lights are normally considered to be a fixed value once the instrument is constructed (Zhang et al. 2009). By contrast, dynamic stray light, which is caused by the scattering of dust particles accumulated on the objective lens surfaces, is variable during the observation. Therefore, a real-time monitor for the dust-scattered stray lights is demanded to guide the cleaning procedure of the optical lens (Elmore 2007).

To assess the dust-scattered light of a coronagraph, many efforts have been put forward. Using the Harvey-Shack BSDF model, Gallagher et al. (2016) simulated the scattering distribution of dust based on the objective lens of the Coronal Solar Magnetism Observatory Large Coronagraph (COSMO-LC), and they showed that the level of dust-scattered stray light at 1.1 solar radii was approximately 3×10^{-6} when the cleanliness level of the objective lens was set to Class-200. Thompson et al. (2003) simulated the dust-scattered stray light level for the COR1 coronagraph on the STEREO satellite, and they found that the overall stray light level increased from 10^{-6} to 10^{-4} as the cleanliness level of the objective lens deteriorated from Class-100 to Class-500. This result demonstrates that the influence of dusts on the objective lens is significant for the overall stray light. Spyak and Jenkins carried out experiments by randomly contaminating a smooth objective lens with polystyrene spheres with diameters ranging from 1 to 85 μm and measured dust-scattering light at a wavelength of 632.8 nm (Spyak & Wolfe 1992a, 1992b; Jenkins et al. 2006). They found that their experiments are very consistent with the modified Mie's scattering theory. Based on the 10 cm coronagraph, NOGIS, located in Lijiang, Sha et al. (2023) imaged dusts on the surface of the objective lens and carefully analyzed the coronal images polluted by the dust-scattered light. They successfully obtained the distribution of scattered light with respect to the heliocentric distance and removed the

effect of dust-scattered light from the coronal images. In the previous work Liu et al. (2023), we performed measurements of dust-scattered stray light levels using an experimental 70 mm inner-occulted coronagraph. By correlating the relative magnitude between ghost images and dust-scattered light, we developed a method to calculate dust-scattered stray light via measuring ghost images, which enables a fast measurement of dust-scattered light levels in a laboratory. Although the aforementioned studies have been conducted on dust-scattered stray light in coronagraphs, a real-time monitor and correction to this type of scattered light during the operation of an instrument remain unresolved.

In the optical system of an inner-occulted coronagraph, the objective lens is directly exposed to sunlight, and thus dusts on its surfaces are the major source of dynamic scattered stray light that affects the quality of the science data of such a coronagraph. During operation of a coronagraph, dusts accumulate on the surfaces of the objective lens, leading to a gradual increase in overall stray light levels. During maintenance of the HAO MK4 coronagraph, Nelson (2006) revealed that the overall stray light level of the instrument can decrease nearly an order of magnitude after dismantling and cleaning the lenses. Furthermore, an increase in dust-scattered stray light can lead to large errors in the inversion of coronal intensity data (Zhang et al. 2022a, 2022b). These studies point out that stray light caused by dusts accumulated on the object lens is a main factor in the stray light level of a coronagraph during its routine operation. Other lenses, such as field lenses, are not directly exposed to sunlight, and scattered lights caused by dust on their surfaces are several orders of magnitude lower than those of the objective lens.

Aiming at real-time monitoring of stray light scattered by dusts on the object lens, in this study we develop a real-time monitoring method for dust-scattered stray light in an inner-occulted coronagraph, namely the Spectral Imaging CoronaGraph (SICG) of the Chinese Meridian Project. The method first simulates the scattering of individual dust particles using micro-pinhole plates and a He–Ne frequency-stabilized laser. By measuring the scattered light from pinhole plates with different diameters, the scattered stray light levels of individual dust particles with various sizes on the image plane of the coronagraph are obtained. These results are then combined with the statistical distribution of dusts on the objective lens surfaces to calculate the total dust-scattered stray light. Its accuracy is then verified by measuring the stray light levels on the coronagraph's objective lens under different cleanliness conditions. In the verifying experiments, a simulated light source is used to illuminate the coronagraph, and the stray light levels are measured under various dust conditions. Image processing techniques are employed to isolate dust-scattered stray light, and the results are compared with those obtained using a statistical method. This method requires only one image of the objective lens for the statistics of the surface dust, making it useful for monitoring dust-scattered stray light during the routine operation of the coronagraph. Additionally, the method focuses on dust-scattered images, and thus it is highly accurate since it is less affected by environmental stray lights.

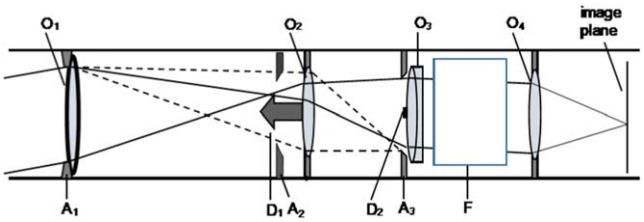

Figure 1. Schematic diagram of the working principle of CMP-II-SICG.

The structure of this paper is outlined as follows. In Section 2, the working principles of the inner-occulted coronagraph are briefly introduced. In Section 3, we describe the structures of a simulated dust scattering device on the objective lens surface and the tests of scattered light from individual dust particles with various diameters. The scattered stray light levels are then calculated based on the statistical distribution of the sizes of dust particles. In Section 4, we first measure the stray light levels under different dust conditions using a test device. Then, we separate the dust-scattered stray light and validate the measurements from Section 3 using the isolated dust-scattered stray light data. Finally, we discuss the sources of error in the dust-scattering statistical measurement method and its significance in practical applications. In Section 5 we provide the conclusions of our study.

2. SICG and Experiment Setup

This study focuses on the SICG which is constructed as part of the second phase of China's Meridian Project (CMP-II). Its working wavelengths are at 637.4 nm and 530.3 nm. The coronagraph features a 200 mm objective lens with a focal length of 2000.2 mm at a wavelength of 637.4 nm and 1983.3 mm at 530.3 nm. It has a field of view ranging from 1.05 to 2 solar radii ($R_{\odot}$). Wavelength selection and switching are achieved through a combination of pre-filters and a four-stage Lyot filter.

The CMP-II/SICG is a typical inner-occulted coronagraph, and its design principle is illustrated in Figure 1. The coronal signal is first imaged by the objective lens O1 onto the field stop A2. The image is then relayed through the remaining lens group to the image plane. The Sun disk is focused by the objective lens O1 onto the inner occulter D1. D1 is designed with an oversized occulter, with an angular diameter that is 1.05 times that of the Sun disk. Diffraction light produced by the aperture stop A1, which is illuminated by direct sunlight, is imaged onto and blocked by the Lyot stop A3. A2 serves as the field stop, determining the instrument's field of view along with D1. Since O1 is directly exposed to sunlight, multiple reflections on its front and rear surfaces generate ghost images.

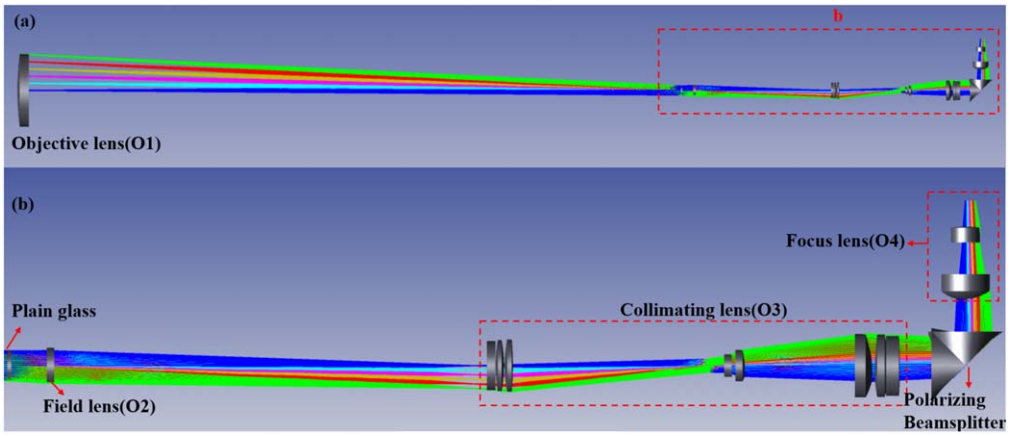

Figure 2. Optical design diagram of the main imaging system and auxiliary imaging path of CMP-II-SICG.

Figure 3. Completed device of CMP-II-SICG.

The field lens O2 re-images these ghost images onto the front surface of the relay lens O3, where they are blocked by the Lyot spot D2. The tunable filter F is used to select specific wavelengths for coronal observation, and the imaging lens O4 re-focuses the output from F onto the image plane.

To enable real-time monitoring of dust-scattered light on the objective lens, the CMP-II-SICG incorporates an auxiliary optical system designed for objective lens imaging, in addition to the traditional inner-occulted coronagraph setup. This auxiliary system, through a beam-splitting optical path, allows simultaneous imaging of both the objective lens surface and the observing objects. As a result, both the coronal image and the dust-scattered light from the objective lens surface can be captured simultaneously. The optical design of the CMP-II-

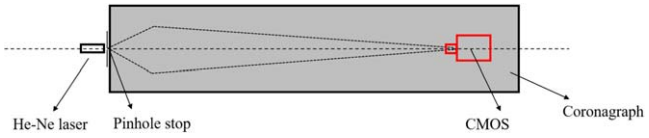

Figure 4. Schematic diagram of the dust-scattering detection system.

SICG is shown in Figure 2, while the actual fabricated device is displayed in Figure 3.

3. Construction and Experiments for the Dust Scattering Measurement System

3.1. The Simulated Dust Measurement System

Since dust particles with various diameters and quantities on the surface of the objective lens have different impacts on the overall stray light level of the coronagraph, the total dust-scattered stray light can be obtained by statistically measuring the number of dust particles on the objective lens surface. Here, the quantitative measurement of the scattered light produced by individual dust particles of different diameters is simulated using a laser-illuminated pinhole. A strong laser beam is used to amplify the scattering from a single dust particle, making it measurable. The simulation system is constructed using a He–Ne frequency-stabilized laser and a set of micro-pinhole plates. The pinholes have various diameters to represent dust particles with different sizes. The laser beam diverging through the pinhole simulates the scattered light produced by individual dust particles when illuminated. The micro-pinhole plates are positioned near the surface of the coronagraph objective lens to simulate the dust scattering effect. The scattered light passes through the coronagraph optical system, reaching the image plane where its intensity is recorded by a detector. The scattered light intensity for each pinhole is then measured and recorded for each pinhole. The measuring process is repeated for various pinhole sizes to simulate the scattered light intensity from different particle diameters. The laser source used here is a highly frequency-stabilized He–Ne laser from REO, equipped with a stabilized power supply, emitting lights at a uniform wavelength of 633 nm. The laser is used to simulate the direct sunlight incident on the coronagraph objective lens. The micro-pinhole plates, manufactured by Thorlabs and Daheng Optics, are made of stainless steel and used to simulate the scattering effect of dusts on the objective lens. The detectors include the Dhyana 95 V2 high-speed CMOS camera from Tucsen Optoelectronics that records imaging data at a very fast frequency, and the back-illuminated CCD camera from Andor that offers low dark current and readout noise for measuring the scattered light intensity at the coronagraph's image plane. A schematic diagram of the dust-scattering detection system is illustrated in Figure 4, and the actual setup is depicted in Figure 5.

3.2. Experimental Procedures and Data Processing

The first part of the simulation experiment involves measuring the intensity of the scattered light from simulated dust. This is achieved by measuring the scattered light intensity at the coronagraph's image plane for dust particles of different diameters, and comparing it with the direct light intensity from the laser source at the image plane. The goal is to determine the level of dust-scattered stray lights for particles with different diameters. The specific procedures are described as follows:

1. In the test, micro-pinhole plates with apertures of 25 μm, 50 μm, 100 μm, 200 μm, and 250 μm are placed in front of the He–Ne frequency-stabilized laser to simulate the scattering from dust particles of different sizes. The laser is mounted on a one-dimensional X-axis translation stage, and its position is shifted at 2 mm intervals from one side of the objective lens surface (objective lens diameter: 200 mm). For each position, a CCD camera records the scattered light intensity at the image plane (with 100 measurements for each simulated dust particle). The average scattered light intensity for each pinhole diameter is noted as I (25–250 μm).
2. After removing the pinhole plates and the coronagraph's inner occulter, a set of neutral density filters is placed in front of the CCD camera to measure the direct light intensity at the image plane, denoted as Iz. The ratio of the scattered light intensity to the direct light intensity is then used to calculate the stray light level L for each simulated dust particle size (25–250 μm).

By comparing the scattered light intensity from simulated dust particles with different diameters, the distribution of simulated dust-scattered stray light levels is obtained, as shown in Figure 6.

From Figure 6, it can be seen that the scattered light intensity at the image plane from smaller dust particles is relatively uniform, whereas larger dust particles exhibit a diffraction ring pattern in their intensity distribution. This occurs because smaller pinholes result in more pronounced diffraction, and for very small diameters, the diffraction effect causes only the zeroth-order component to appear, leading to a more uniform intensity distribution. As the aperture size increases, the diffraction rings become denser, and more fringes appear at the image plane.

In the data processing, two averaging steps were employed. First, the scattered light from dust particles was measured at 100 different positions, and the average scattered intensity for a single particle size was obtained. This approach facilitates the statistical distribution calculation that follows. In reality, the dust-scattered light at the image plane is a statistical accumulation of scattered light from dust particles of varying sizes and positions. After the statistical accumulation, the dust-scattered light can be considered approximately uniform at the

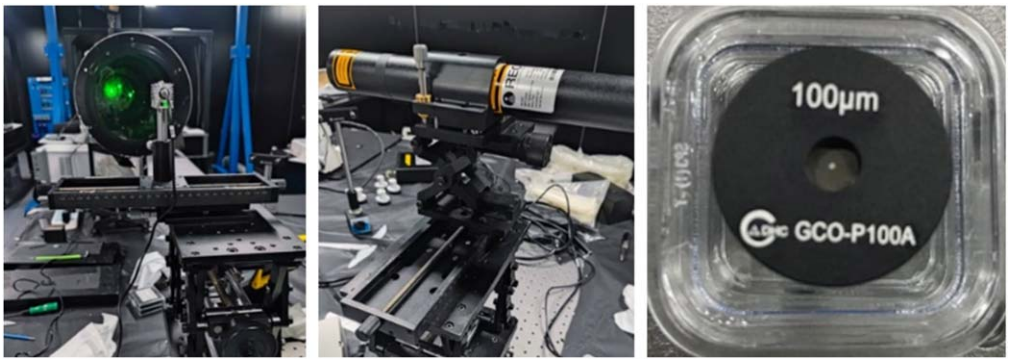

Figure 5. Actual setup of the dust-scattering detection system. The left image shows the calibration of the laser pointing toward the coronagraph, the center image displays the He–Ne frequency-stabilized laser source used for simulating dust, and the right image features the pinhole plates used to simulate dust scattering.

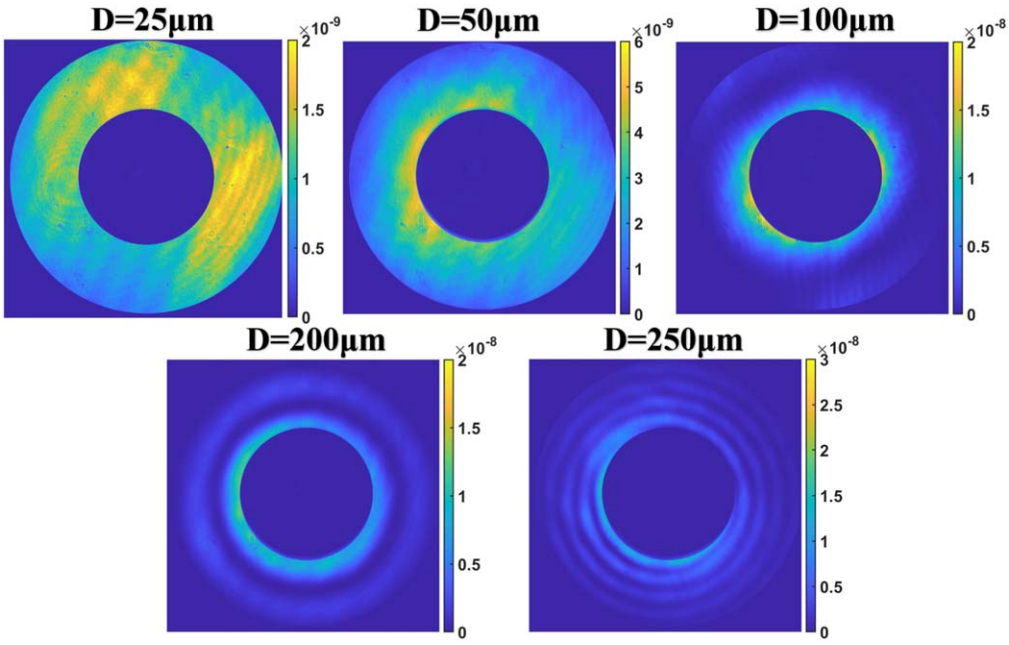

Figure 6. Distribution of stray light levels for simulated dust particles of different diameters.

image plane, making this averaging step statistically reasonable. Second, after averaging the scattered light distribution at the image plane, another averaging step was performed. This study does not aim at considering the intensity distribution of individual dust particles but instead calculates the average scattered intensity at the image plane, using this as an indicator for monitoring the dust accumulation on the objective lens. After applying the two rounds of averaging to the stray light distribution values from different simulated dust particles as exampled in Figure 6, the average stray light levels L for simulated dust particles of different diameters were calculated as 1.02×10^{-9} (25 μm), 2.06×10^{-9} (50 μm), 4.57×10^{-9} (100 μm), 7.8×10^{-9} (200 μm), and 9.66×10^{-9} (250 μm), while the corresponding standard deviations are 1.33×10^{-10}(25 μm), 2.53×10^{-10}(50 μm), 4.39×10^{-10}(100 μm), 1.40×10^{-9}(200 μm) and 7.67×10^{-10}(250 μm). The fitted curve of the relationship between the stray light level L and the particle diameter D for individual simulated dust particles is plotted in Figure 7.

From Figure 7, it can be seen that the relationship between the stray light level L at the image plane for simulated dust particles and their corresponding diameter D, as determined by fitting the sample points, is described by the following formula: $L = 3.57 \times 10^{-16} \times \mathrm{D}^3 - 1.87 \times 10^{-13} \times \mathrm{D}^2 + 6.53 \times 10^{-11} \times \mathrm{D} - 5.97 \times 10^{-10}$. This function can be used to directly calculate the stray light level for dust particles of different diameters. Once the number of dust particles of various sizes on the actual surface of the coronagraph's objective lens is statistically

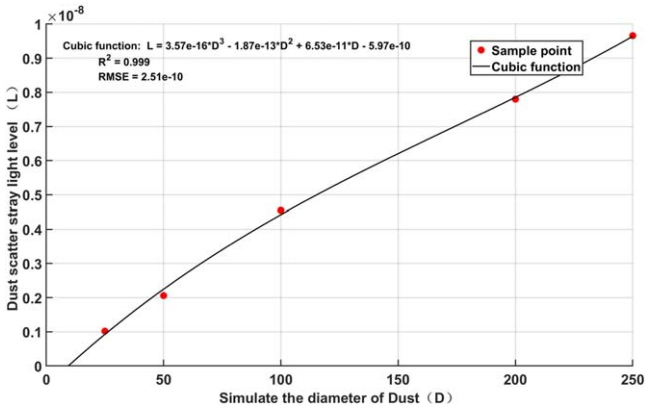

Figure 7. Curve of simulated dust stray light level L vs. corresponding diameter D.

determined, the total dust-scattered stray light level on the lens surface can be calculated by combining these results with the simulated dust stray light levels.

The second part of the simulation experiment involves using dust particles of known diameters to calibrate the diameter of dust on the coronagraph's objective lens. Since the size of the dust particles appears as a certain number of pixels on the detector during imaging, it is necessary to establish a relationship between the number of pixels occupied by the dust in the image and the actual diameter of the dust on the objective lens. A 100 μm pinhole plate is used to simulate the dust for calibration. The CMOS camera captures multiple images of the 100 μm simulated dust on the objective lens, and these images are averaged for further analyses. The intensity distribution along the X-axis of the image, corresponding to the 100 μm simulated dust scattering point, is then normalized to obtain an intensity distribution curve, as shown in Figure 8.

From the intensity distribution curve, we can see that it is advantageous to select the position where the normalized intensity reaches 1% as the threshold for determining the edge of the dust-occupied area. The number of pixels occupied by the 100 μm simulated dust on the CMOS camera is 14 pixels along X-axis. This corresponds to each pixel representing a size of 7.14 μm on the objective lens surface. Subsequently, after imaging the coronagraph's objective lens and obtaining the dust scattering point distribution, the diameter of the dust particles on the lens surface can be calculated. After that, by removing the simulated dust setup, a uniform white light source is used to illuminate the objective lens. Using the same CMOS camera, an image of the dust particles on the objective lens surface is captured, as shown in Figure 9.

Additionally, we examine the shape of the dust on the objective lens surface projected onto the image plane. From the dust image on the objective lens surface, four dust particles of different diameters (indicated by the red boxes labeled as 1-4 in Figure 9) were selected for diameter calculation. The dust intensity along the X-axis was normalized at the center of each particle, and the corresponding intensity distribution curves were generated. These intensity distribution curves are shown in Figure 10. From the images, it is evident that the intensity distribution of individual dust scattering points follows a pattern of strong intensity at the center, tapering off toward the edges. Using a threshold at 1% of the normalized intensity, we define the boundary of each dust particle and we find the number of pixels occupied by Dust 1-4 was measured as 13.0 pixels, 15.0 pixels, 20.0 pixels, and 30.0 pixels, respectively. Based on the calibration results, the diameters of Dust 1-4 on the objective lens surface were calculated as 93 μm, 107 μm, 143 μm, and 214 μm respectively. By extending this diameter calculation across the entire dust image on the objective lens surface, the statistical distribution of dust particles of different diameters on the coronagraph's objective lens can be obtained.

The statistical counting of dust particles of different diameters on the objective lens surface is achieved through image processing of the dust image in Figure 9. The corresponding steps are as follows. First, dark field subtraction is applied. Second, a background threshold is set to subtract the background light, minimizing its impact on the dust scattering point count. Finally, a binarization process is applied, where the dust scattering point regions are assigned a value of 1, and all other areas are set to 0. This approach simplifies the subsequent statistical analysis. The original image of dust scattering from the objective lens surfaces and the binarized image used for statistical analysis are shown in Figure 11.

By combining the binarized image of the dusts with the statistical values of their number and area, the number of dust particles of different diameters can be calculated, which in turn allows the determination of the dust-scattered light levels. First, the binarized image is processed by segmenting the data to calculate the number of pixels occupied by each independent scattering point. The scattering points are then sorted based on the area they occupy in terms of pixel count, facilitating further analysis. Each scattering point is approximated as a circular shape, and the equivalent diameter of each dust particle is obtained. The diameter of the dust particles on the objective lens is then determined by applying the formula obtained from Figure 7. The number of dust particles with different diameters is statistically analyzed, and their diameter distribution is obtained. Finally, by correlating the dust particle diameter statistics with the simulated dust scattering light levels, the current level of dust-scattered stray light on the objective lens is achieved. In Figure 12, we show the area-labeled image of the dust scattering points, and the histogram distribution of the dust diameters obtained in the experiment is shown in Figure 13.

From Figure 13, it can be seen that most of the dust particles on the objective lens have diameters under 100 μm, with a smaller fraction in the range of 100–200 μm, and only a few particles exceeding 200 μm. The larger dust particles are likely

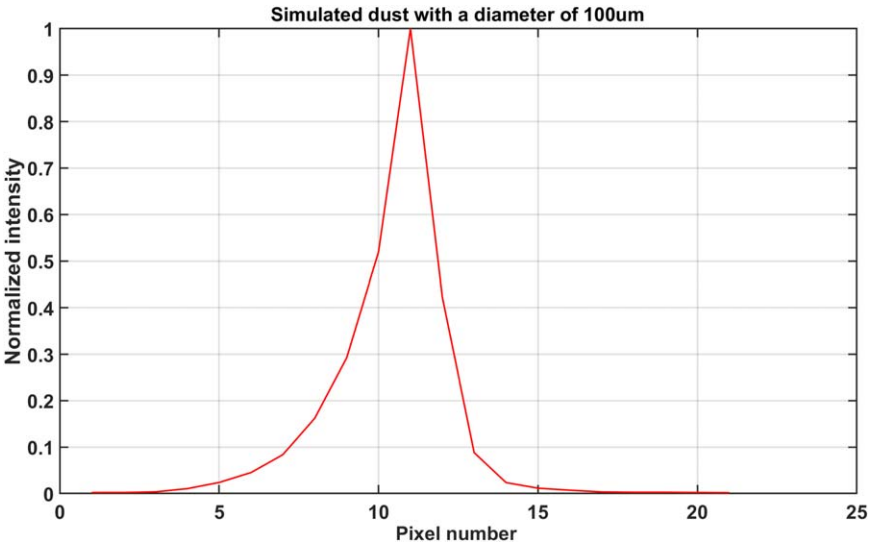

Figure 8. Normalized intensity distribution of 100 μm simulated dust.

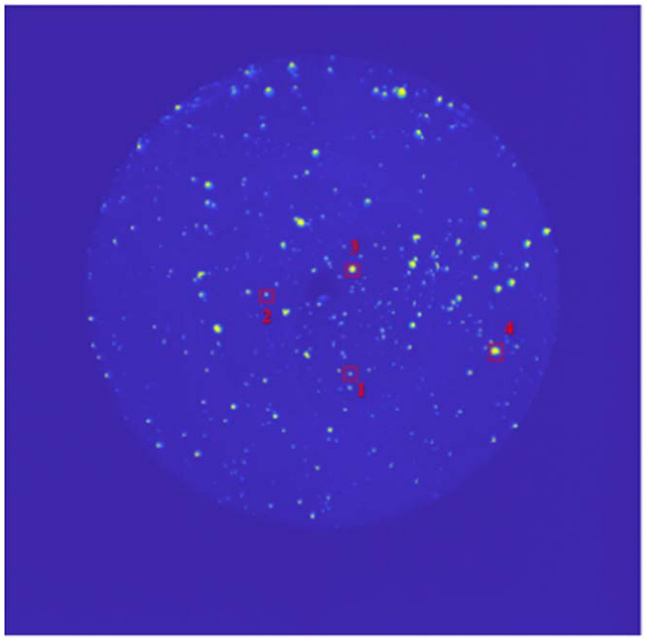

Figure 9. Dust imaging on the surface of the coronagraph's objective lens.

due to improper cleaning processes (e.g., large particles left behind due to incomplete air-blowing during cleaning). By multiplying the number of dust particles N for each diameter range by the corresponding stray light level obtained from the previous simulations, the current total dust-scattered stray light level on the objective lens surface is calculated to be 1.63×10^{-6}.

4. Experimental Validation

The accuracy of the dust scattering statistical measurement method is validated by measuring the stray light levels under different dust conditions on the coronagraph's objective lens surfaces. The statistical measurement method described in Section 3 was applied to different dust conditions on the objective lens, and the corresponding dust-scattered stray light levels were calculated for varying cleanliness levels. The objective lens of the coronagraph was disassembled in the laboratory and placed face-up (with the external surface of the objective lens facing the Sun). It was left undisturbedly in the laboratory for accumulation of dusts for periods of 1, 2, 4 and 8 hr. After each period of exposure, the objective lens was reassembled onto the coronagraph, and the dust distribution was imaged using a CMOS camera. The dust conditions on the objective lens were recorded as LV1, LV2, LV3, and LV4, where LV1, LV2, LV3, and LV4 represent the dust conditions after 1, 2, 4, and 8 hr of exposure, respectively. The dust distribution on the objective lens surface after 1, 2, 4, and 8 hr of exposure in a cleanroom environment is shown in Figure 14, and the statistical results of the dust conditions are presented in Figure 15.

From the statistics shown in Figure 15, we can see that dust particles with diameters between 0 and 100 μm are the most affected by the accumulation time. Dust particles with the other diameters showed only slight increases or remained nearly constant while the accumulation time increases. This is possibly due to the laboratory environment that is a Class-1000 cleanroom, where larger dust particles are scarce. Based on the dust particle counts from Figure 15 and the dust-scattered stray light levels obtained from the simulations, the

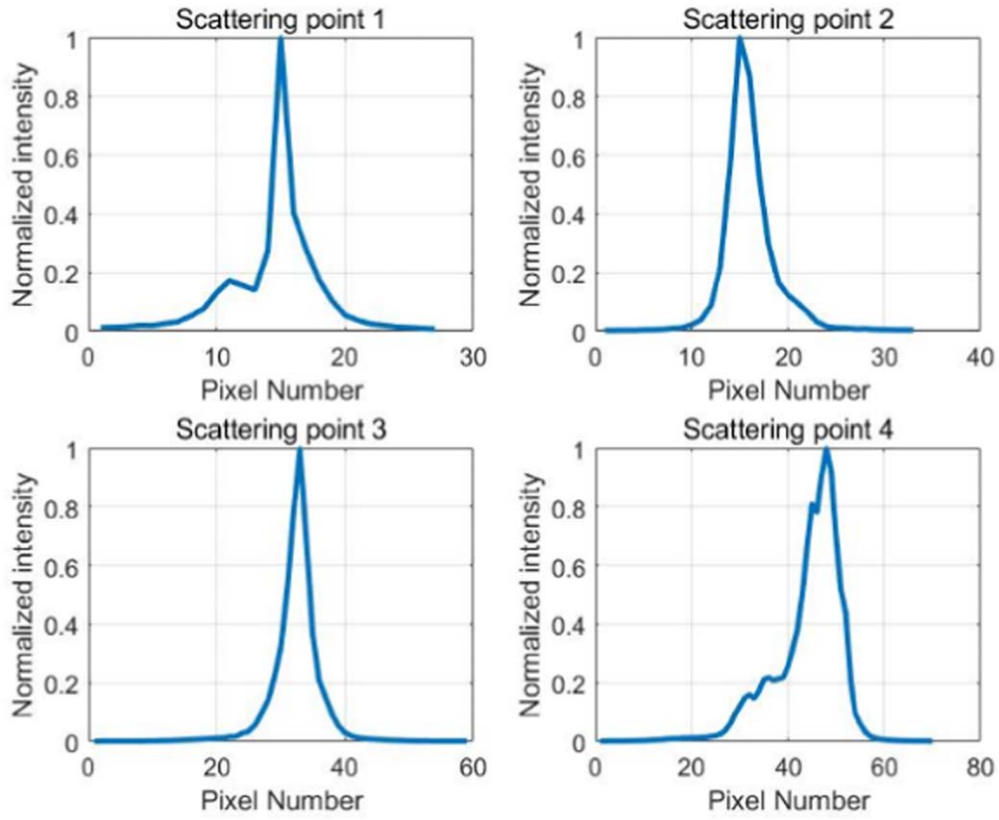

Figure 10. Normalized intensity distribution of four dust particles with different diameters on the objective lens surface.

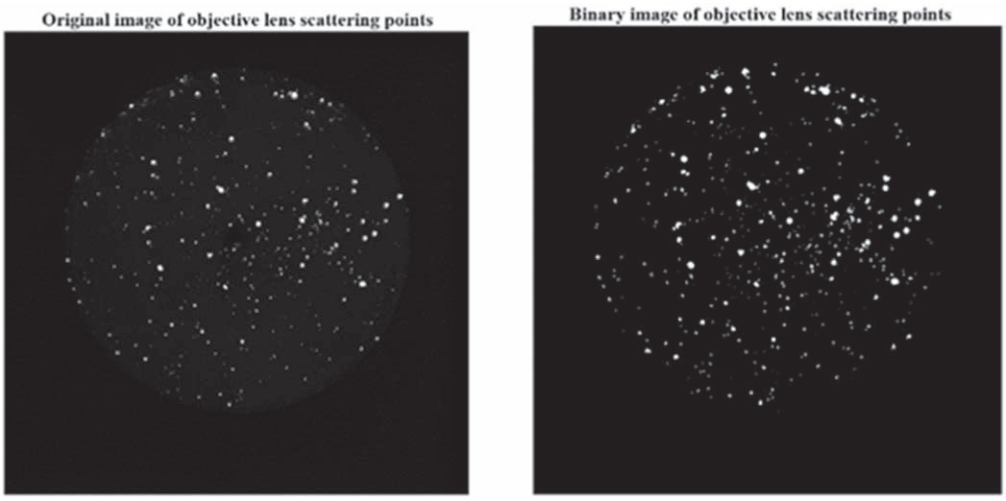

Figure 11. Original dust image (left) and binarized image for statistical analysis (right).

stray light levels corresponding to dust conditions of LV1–LV4 on the objective lens were obtained to be 1.75×10^{-6}, 1.79×10^{-6}, 1.83×10^{-6}, and 1.98×10^{-6}, respectively.

The measurement of stray light levels under different dust conditions on the surface of the coronagraph's objective lens is performed using the coronagraph's stray light measurement system. This system is based on the traditional stray light

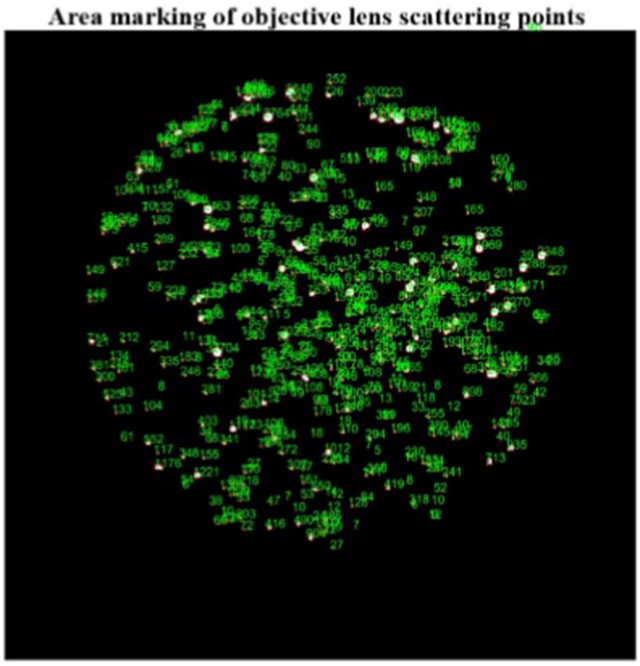

Figure 12. Area-labeled image of dust scattering points (green numbers indicate the area of each scattering point).

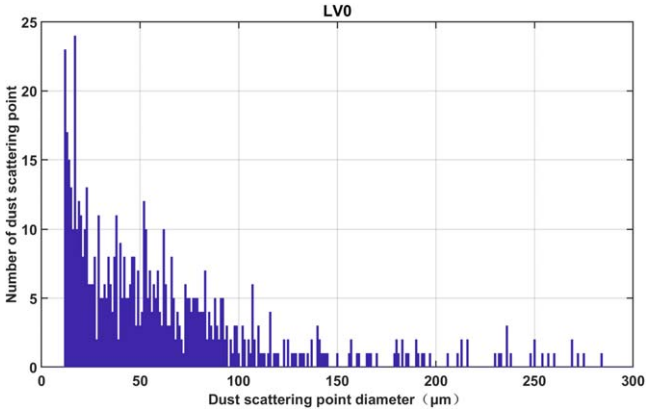

Figure 13. Histogram of dust scattering point diameter distribution.

measurement setup for inner-occulted coronagraphs (Liu et al. 2023). The measurement process is as follows. First, the overall stray light levels for the coronagraph's objective lens are measured under various dust conditions. A CCD camera is placed at the image plane of the coronagraph, and the stray light intensity at the image plane, I0 to I4, is recorded for each condition. Next, the internal occulter is removed, and a neutral density filter set is inserted to measure the direct light intensity Iz. By combining the recorded stray light intensity and the direct light intensity, the total stray light levels, SL0 to SL4 (SL0 is that measured immediately after the cleaning of the objective lens is done), are obtained. Since the stray light measurements provide a two-dimensional matrix of the coronagraph's total stray light levels across the field of view, the stray light levels are averaged radially from the center of the field outward. This produces the coronagraph's stray light levels at different locations in the field of view, as shown in Figure 16.

From Figure 16, we can observe that the increase in dust from LV0 to LV4 on the objective lens surface leads to a rise in the coronagraph's stray light levels. However, the relative increase is small compared to the overall stray light levels. This is due to the high cleanliness of the laboratory's Class 1000 cleanroom environment. Compared to the stray light level for the LV0 dust condition, the stray light level for the LV4 condition shows an average increase of 3×10^{-7}, which is consistent with the stray light level increment calculated using the dust scattering statistical measurement method. This increment accounts for approximately 10% of the initial average stray light level of the coronagraph's objective lens. Therefore, when the coronagraph's objective lens is left exposed for an extended period of time, the increase in dust-scattered stray light can significantly affect the overall stray light level. This effect would be much more pronounced when the coronagraph operates at the observatory site (i.e., an outdoor environment).

Since the stray light levels on the coronagraph's image plane are positively correlated with the stray light intensity at the Lyot stop (Liu et al. 2023), a method is employed to effectively distinguish between dust-scattered light and other stray light by separating their respective intensities at the Lyot stop. The specific separation method is as follows: The conjugate image of the objective lens at the Lyot stop is analyzed. Dust-scattered light appears as highly focused scattering points at the Lyot stop, while other types of stray light are more uniformly distributed. By using image processing techniques, the intensities of dust-scattered stray light and other stray light at the Lyot stop can be separated, and their relative contributions are calculated. These correspond to the contributions of both types of stray light at the image plane of the coronagraph. For example, the separated intensity image of dust-scattered stray light and other stray light at LV0 of the objective lens is shown in Figure 17.

After summing the separated intensities of the two types of stray light and dividing them by the total intensity before separation, we determined that dust-scattered stray light accounts for 55% and other stray light for 45% of the total. Using the total stray light level under the LV0 condition from Figure 16, the average level of dust-scattered stray light can be calculated as: $0.55 \times SL_0 = 1.58 \times 10^{-6}$. Since the increase in stray light from LV1 to LV4 is solely due to dust accumulation on the objective lens, while the other types of stray light remain constant, the difference in total stray light levels between LV1 and LV4 and LV0 can be attributed to dust-scattered stray lights. Thus, the dust-scattered stray light level under the LV0

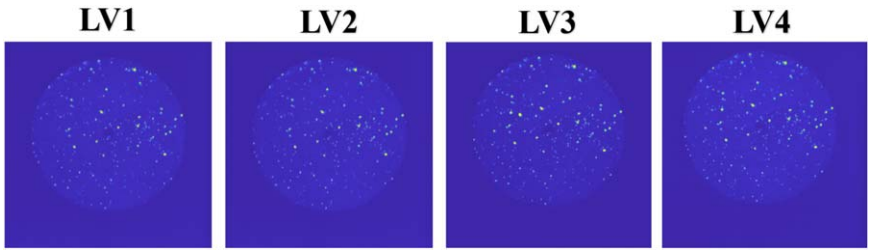

Figure 14. Dust distribution on the surface of the coronagraph objective lens after 1, 2, 4, and 8 hr of exposure in the laboratory.

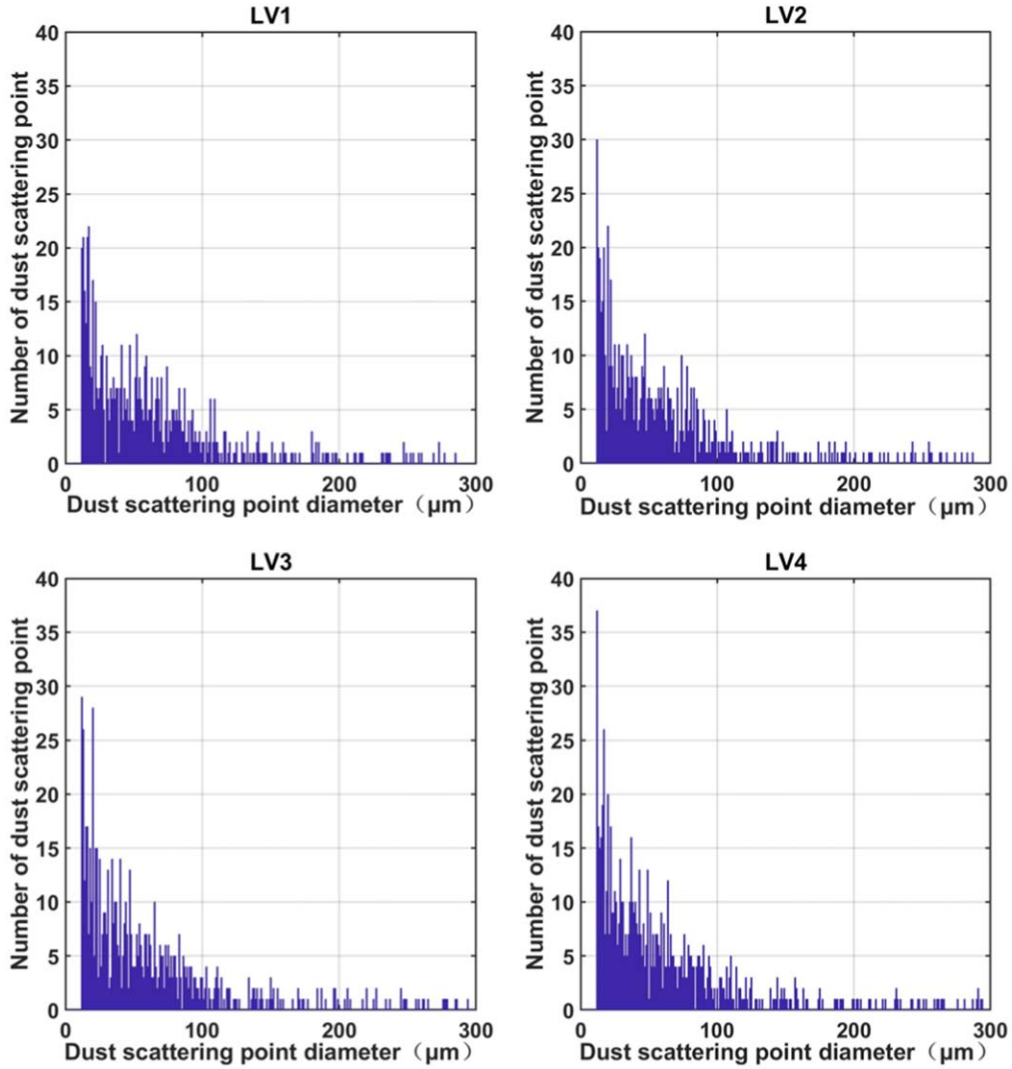

Figure 15. Statistical chart of the dust conditions on the surface of the coronagraph's objective lens after 1, 2, 4, and 8 hr of exposure in the laboratory.

condition serves as the initial value. By adding the difference in total stray light levels between LV1 and LV4 and LV0 to the initial value, the dust-scattered stray light levels for LV1–LV4 are obtained as: 1.67×10^{-6}, 1.77×10^{-6}, 1.82×10^{-6}, and 1.97×10^{-6} respectively, which are very consistent with the values obtained by our aforementioned method (see Table 1).

As shown in Table 1, the differences in dust-scattered stray light levels between the two methods are around 2%, indicating

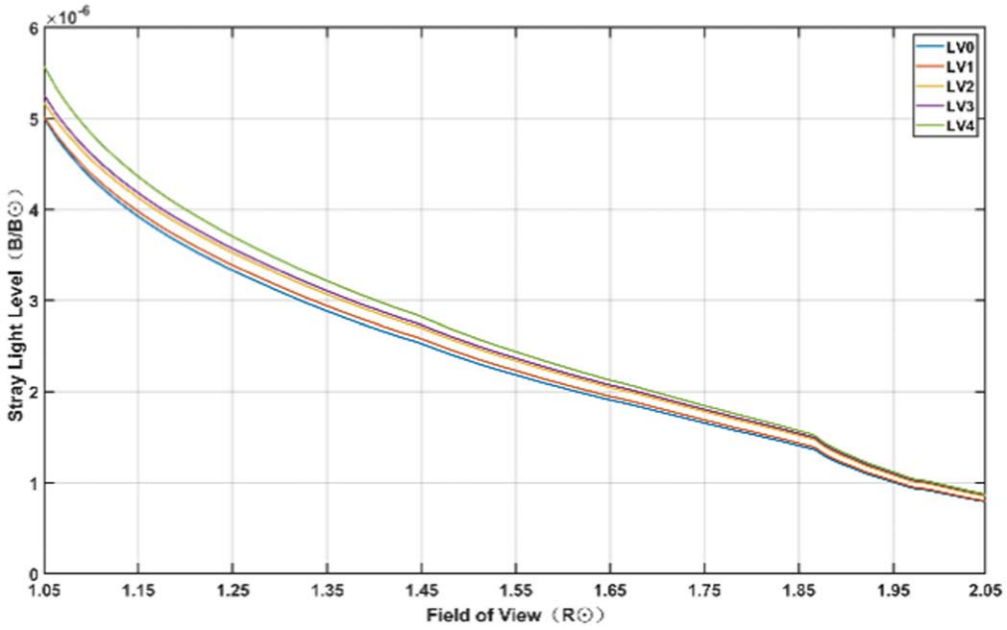

Figure 16. Stray light levels of the coronagraph corresponding to different dust conditions on the objective lens surface.

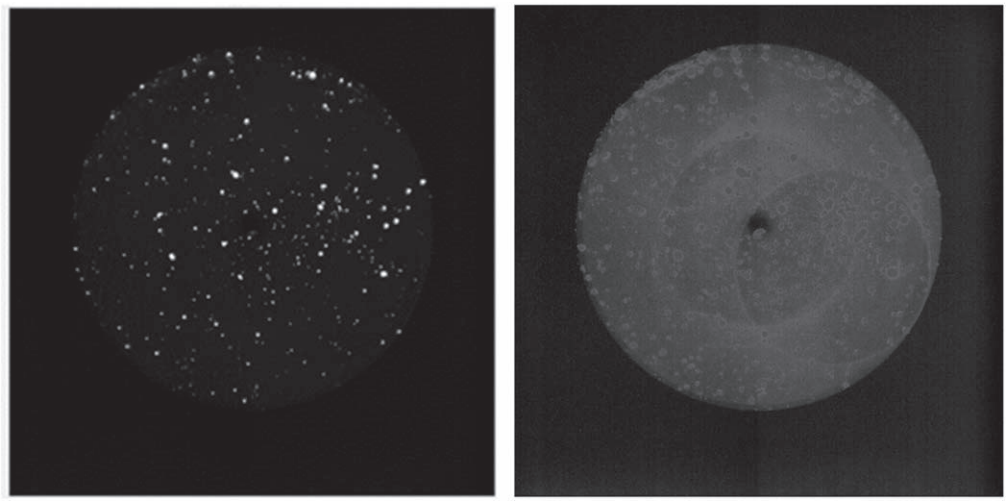

Figure 17. Intensity separation of dust-scattered stray light (left) and other stray light (right) at the Lyot stop.

Table 1
Comparison of Dust-scattered Stray Light Levels Obtained by the Dust Scattering Statistical Measurement Method and the Stray Light Detection Method

Objective Lens Dust Condition (LEVEL)	Dust Scattering Statistical Measurement Method Stray Light Level	Stray Light Detection Method Stray Light Level	Relative Error (Percentage)
LV0	1.63×10^{-6}	1.58×10^{-6}	3.1%
LV1	1.75×10^{-6}	1.67×10^{-6}	4.6%
LV2	1.79×10^{-6}	1.77×10^{-6}	1.1%
LV3	1.83×10^{-6}	1.82×10^{-6}	0.5%
LV4	1.98×10^{-6}	1.97×10^{-6}	0.5%

a good correspondence between the results. This demonstrates the accuracy and effectiveness of the method based on dust scattering statistics. Several factors may contribute to the observed discrepancies.

1. Measurement error from simulated dust: the simulated dust measurements were conducted using standard circular pinhole plates that cannot perfectly simulate real dust particles. This may lead to some measurement errors when correlating the simulated dust results with real dust particles.
2. Error in the relation between real size of a dust particle and its occupancy on the imaging plane: The dust scattering levels were measured using only five standard pinhole diameters, μm, 50 μm, 100 μm, 200 μm, and 250 μm. To obtain the scattering levels for other diameters, data interpolation and fitting were applied. Since the number of fitting sample points was limited, this introduces error into the fitting function. Custom-designed pinhole plates with additional diameters could be useful for improving the accuracy of the fitting function and thereby enhancing the precision of the measurement method.
3. Error from stray light detection of the coronagraph: In the stray light detection processes, environmental stray light and fluctuations in the intensity of the simulated solar light source could have introduced some detection errors in the overall stray light levels of the coronagraph, which in turn affected the measurement of dust-scattered stray light. Improvements could be made by enhancing the cleanliness of the detection environment, measuring and correcting for the effects of environmental stray light, and calibrating the intensity fluctuations of the simulated solar light source. These steps would reduce detection errors and improve the accuracy of dust-scattered stray light measurements.
4. When the instrument is deployed in an outdoor environment (e.g., in Lijiang), environmental dust of various diameters may accumulate on the objective lens. For dust particles smaller than 25 μm, their contribution to the overall stray light is minimal and can be approximated as negligible. For dust particles larger than 250 μm, however, their significant impact on the coronagraph's overall stray light necessitates cleaning the objective lens to prevent the accumulation of such large-diameter dust.

Although the aforementioned factors may introduce some measurement errors to the dust scattering statistical method, we find they do not affect the overall effectiveness of this method in monitoring dust-scattered stray light when it is tested under different dust conditions. The dust scattering statistical method simplifies the complex laboratory measurements of dust-scattered stray light into a more manageable process of measuring the number and diameter of dust particles on the objective lens surface.

5. Summary

This paper presents the dust scattering statistical method for monitoring the dust-scattered stray light levels on the objective lens of a coronagraph through statistical measurement of dust particles on the lens surface. The method calculates the dust-scattered stray light level by correlating measurements of simulated dust with the real dust conditions on the objective lens. Experimental validation was conducted using stray light level measurements under different dust conditions on the objective lens. The dust-scattered stray light levels on the objective lens of CMP-II/SICG measured using this method ranged from 1.6×10^{-6} to 2×10^{-6} for various cleanliness conditions. The validation experiments showed that the differences between the measured dust-scattered stray light levels and the calculated values from this method were about 2%, giving strong confidence for the method's effectiveness and accuracy. This method provides a handy tool to monitor the dust level of the objective lens of SICG and guides the cleaning routine. The method has been applied to the instrument at the observing site and has significantly improved the efficiency of the stray light control pipeline.

Acknowledgments

This work is supported by National Natural Science Foundation of China (grant Nos. 42274227, 41904168, U1931122), National Key R&D Program of China No. 2021 YFA0718600, and the Chinese Meridian Project (CMP).

References

Elmore, D. 2007, COSMO Technical Note, 10, 1–8
Gallagher, D., Wu, Z., Larson, B., et al. 2016, Proc. SPIE, 54, 9906
Huang, Y., Zhang, H., Ding, Y., & Wang, T. 2023, AcPSi, 52, 1122003
Jenkins, D., Fest, E., Kremer, R., & Spyak, P. 2006, Proc. SPIE, 6291, 55
Liu, D., Zhang, H., Sun, M., et al. 2023, RAA, 24, 025020
Nelson, P. 2006, COSMO Technical Note, https://opensky.ucar.edu/system/files/2024-09/reports_12.pdf, 4, 1–28
Sha, F., Liu, Y., Zhang, X., & Song, T. 2023, SoPh, 298, 11
Spyak, P. R., & Wolfe, W. L. 1992a, OptEn, 31, 1764
Spyak, P. R., & Wolfe, W. L. 1992b, OptEn, 31, 1775
Su, D. 1959, JNUNS, 01, 24
Thompson, W., Davila, J., Fisher, R., et al. 2003, Proc SPIE, 4583, 11
Zhang, H.-X., Lu, Z., Xia, L.-D., Liu, H., & Li, P. 2009, Optics and Precision Eng., 17, 2371
Zhang, X.-F., Liu, Y., Zhao, M.-Y., et al. 2022a, RAA, 22, 075007
Zhang, X.-F., Liu, Y., Zhao, M.-Y., et al. 2022b, RAA, 22, 075012